A&A 502, 599–603 (2009)
DOI: 10.1051/0004-6361/200811359
© ESO 2009

Astronomy & Astrophysics

Heavy ion irradiation of condensed CO_2: sputtering and molecule formation

E. Seperuelo Duarte[1,2,3], P. Boduch[1], H. Rothard[1], T. Been[1], E. Dartois[4], L. S. Farenzena[5], and E. F. da Silveira[2]

[1] Centre de Recherche sur les Ions, les Matériaux et la Photonique (CEA /CNRS /ENSICAEN /Université de Caen–Basse Normandie), CIMAP – CIRIL – Ganil, Boulevard Henri Becquerel, BP 5133, 14070 Caen Cedex 05, France
e-mail: esduarte@ganil.fr, esduarte@gmail.com
[2] Physics Department, Pontifícia Universidade Católica, Rua Marquês de S. Vicente 225, 22453-900 Rio de Janeiro, Brazil
[3] Grupo de Física e Astronomia – CEFET/Química de Nilópolis, Rua Lúcio Tavares 1045, Centro, 26530-060 Nilópolis, Brazil
[4] Institut d'Astrophysique Spatiale, Astrochimie Expérimentale, UMR-8617 Université Paris-Sud, bâtiment 121, 91405 Orsay, France
[5] Physics Department, Universidade Federal de Santa Catarina, Florianópolis, SC, Brazil

Received 16 November 2008 / Accepted 28 April 2009

ABSTRACT

Context. Ices present in different astrophysical environments are exposed to ion irradiation from cosmic rays (H to heavier than Fe) in the keV to GeV energy range.
Aims. The objective of this work is to study the effects produced in astrophysical ices by heavy ions at relatively high energies (MeV) in the electronic energy loss regime and compare them with those produced by protons.
Methods. $C^{18}O_2$ was condensed on a CsI substrate at 13 K and it was irradiated by 46 MeV $^{58}Ni^{11+}$ up to a final fluence of 1.5×10^{13} cm^{-2} at a flux of 2×10^9 cm^{-2} s^{-1}. The ice was analyzed in situ by infrared spectroscopy (FTIR) in the 5000–600 cm^{-1} range.
Results. The CO_2 destruction was observed, as well as the formation of other species such as CO, CO_3, O_3, and C_3. The destruction cross section of CO_2 is found to be 1.7×10^{-13} cm^2, while those for the formation of CO, CO_3, and O_3 molecules are 1.6×10^{-13} cm^2, 4.5×10^{-14} cm^2, and 1.5×10^{-14} cm^2, respectively. The sputtering yield of the CO_2 ice is 4.0×10^4 molecules/impact, four orders of magnitude higher than for H projectiles at the same velocity. This allows us to estimate the contribution of the sputtering by heavy ions as compared to protons in the solar winds and in cosmic rays.
Conclusions. The present results show that heavy ions play an important role in the sputtering of astrophysical ices. Furthermore, this work confirms the quadratic stopping power dependence of sputtering yields.

Key words. molecular data – molecular processes – methods: laboratory – techniques: spectroscopic

1. Introduction

Interstellar ice grain mantles consist of small molecules containing hydrogen, carbon, nitrogen and oxygen atoms. In the solar system, condensed gases are also found in comets, rings, and cold satellites. Among the interstellar ices, H_2O, CO, and CO_2 are the most abundant materials (e.g. van Dishoeck 2004; Gibb et al. 2004; Dartois 2005; Pontoppidan et al. 2008). Therefore, these particular ices are widely studied (Jenniskens & Blake 1994; d'Hendecourt & Allamandola 1986; van Broekhuizen et al. 2006; Wood & Roux 1982; Ehrenfreund et al. 1996; Falk 1986). The occurrence of molecular synthesis in these astrophysical ices by cosmic rays, solar wind, UV radiation, and electron collision has been the object of research over the last decades (e.g. Hudson & Moore 1999; Palumbo et al. 1998; Ponciano et al. 2005; Farenzena et al. 2005; Gerakines et al. 2000; Baragiola et al. 2008; Lafosse et al. 2006). Ion beam irradiation leads to energy deposition on electrons (electronic stopping power) and on the target nuclei (nuclear stopping power). This in turn causes on the one hand the ejection of particles (electron emission, sputtering of neutrals and ions), and, on the other hand, material modification (chemical reactions and phase changes). Here, we focus our study on high energy particles in the electronic energy loss regime. In space, this kind of particles is present in interstellar cosmic rays (e.g. Webber & Yushak 1983; Boezio et al. 1999) and in other astrophysical objects or phases, like protoplanetary disks, stellar winds and supernovae shocks (e.g. Jones et al. 1996, 2000).

The formation of solid CO_2 and its evolution are still under debate in the literature (Roser et al. 2001; Pontoppidan et al. 2008). Laboratory experiments show that CO_2 can be formed from a CO ice when it is exposed to UV, and also by ion irradiation (Loeffler et al. 2005; Jamieson et al. 2006; d'Hendecourt et al. 1986; Grim et al. 1989; Allamandola et al. 1997; Gerakines et al. 1996; Moore et al. 1991). The opposite situation also occurs: CO is produced when a CO_2 ice is irradiated by energetic particles (Strazzulla et al. 2005). The energetic particle abundance (mainly H to Fe) in cosmic rays and solar wind has been the subject of research to understand their production mechanisms and their effects on cosmic bodies (Mewaldt et al. 2007). Although the flux of Fe nuclei is three orders of magnitude lower than that of protons, their effects may play an important role because they are multicharged and their stopping power in matter may be up to two orders of magnitude higher. In order to understand the effects of swift heavy ions on ice, it is necessary to measure their sputtering yields and reaction cross sections and then compare them to those caused by H flux. Here, we present first Fourier Transform InfraRed (FTIR) measurements of condensed $C^{18}O_2$ irradiated by heavy projectiles at high energies (46 MeV $^{58}Ni^{11+}$) for which the electronic energy loss

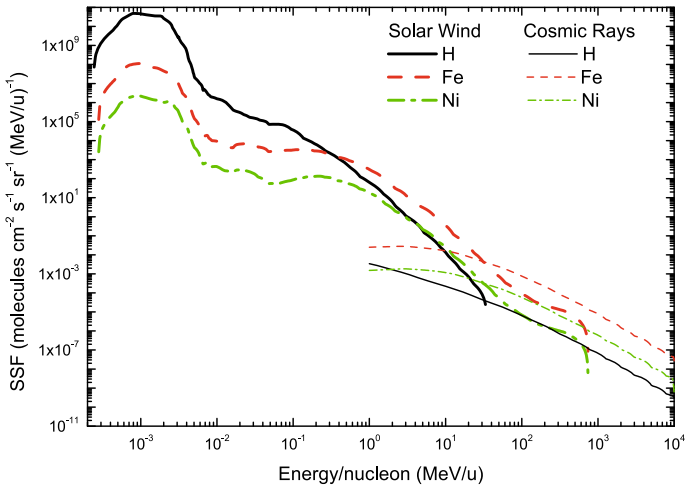

Fig. 1. Specific sputtering flux for H, Fe, and Ni ions in solar wind and cosmic rays. Ions are supposed to be in their respective charge states.

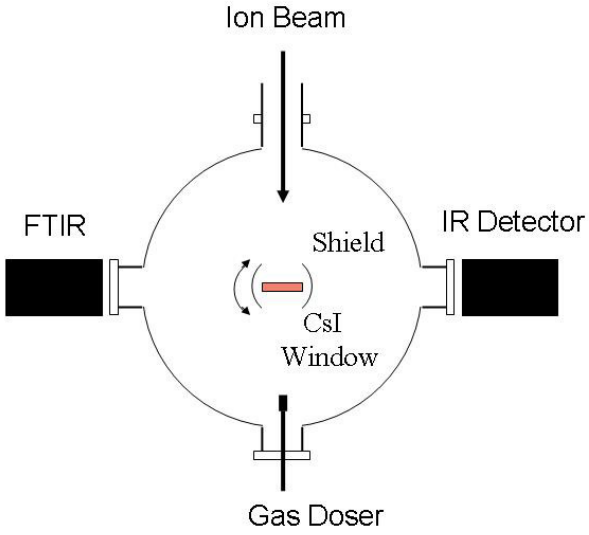

Fig. 2. A schematic representation of the experimental set-up. The ion beam impinges perpendicularly on the thin film ice deposited on a CsI disk. After partial irradiation, the target is rotated 90° for FTIR analysis.

dominates. For the same velocity, the target ionizing effects of Ni and Fe projectiles are almost identical.

In space, protons are the most abundant ions present in the solar wind and galactic cosmic rays. Mewaldt et al. (2007) measured the velocity distribution of helium, oxygen, and iron fluences in the solar wind. The data cover a velocity range from 10^2 eV/u to 10^9 eV/u. For the galactic cosmic rays, Shen et al. (2004) calculated velocity distributions for proton, oxygen, and iron fluxes. The velocity range was from 10^6 eV/u to 10^{11} eV/u. In both environments, the proton abundance is three orders of magnitude higher than iron abundance. However, the sputtering produced by these particles is velocity dependent. To compare the contribution of protons and heavy ions to sputter ices in astrophysical environments, the specific sputtering flux (SSF), defined as the product of each ion flux in cosmic rays and solar wind by its corresponding sputtering yield on ice, should be considered. Using the relation $Y \sim S_e^2$, with $S_e = (dE/dx)_e$ being the electronic stopping power, found by Brown et al. (1982) and supported by the present experimental data, Y was calculated as a function of projectile velocity using SRIM. The SSF as a function of velocity squared is presented in Fig. 1 for solar wind particles as well as for galactic cosmic rays. The ratio between Ni and Fe was taken from Karrer et al. (2007).

For solar wind particles, the specific sputtering flux can be divided in two regions: (i) for squared velocities lower than 0.3 MeV/u, the SSF produced by protons is dominant; and (ii) for higher velocities, heavy ions become more important. In the case of cosmic rays in dense clouds, the SSF of heavy ions are dominant in the whole velocity range considered. Therefore, further studies of swift heavy ions irradiation on astrophysical ices are need.

2. Experimental

The sketch of the experimental set-up is presented in Fig. 2. The 46 MeV $^{58}Ni^{11+}$ ion projectiles produced by the IRRSUD beamline of the heavy ion accelerator GANIL (Grand Accélérateur National d'Ions Lourds) impinge perpendicularly to the ice target. The procedure to ensure a precise dosimetry (determination of the ion flux within ±10%) is as follow: the ion beam is swept horizontally and vertically by means of sweeping magnets. These are operated with saw tooth shaped pulses at very different frequencies (about 3 Hz and 300 Hz) in order to homogenously distribute the single ion impacts over the irradiated surface. A set of slits, situated between the sweeping device and the target, allows measurement of the current and thus the number of ions stopped by the slits. A Faraday cup can be inserted in front of the target and allows measurement of the number of ions that would impact on the target. Since the swept ion beam radiation field is homogenous, the ratio of the current measured on the slits and in the Faraday cup is constant (even if variations in the absolute intensity of the beam occur). When the Faraday cup is removed and the beam impinges on the target, the flux of ions can thus be calculated from the ion beam current measured on the slits.

The thin ice film was prepared by condensation of $C^{18}O_2$ gas (purity 97.7%, Euriso-top) onto a CsI substrate. The ^{18}O isotope-enriched ice was selected because, on the one hand, its chemistry is expected to be the same as that of ^{16}O, and on the other hand, experiments with H_2O+CO_2 ice are planned in the near future and labeled compounds are useful to follow the chemical reactions on the target. The thermal contact with the holder is maintained by indium rings. The copper holder is attached to a closed-cycle helium cryostat. The system is situated in a high-vacuum chamber ($p \approx 4 \times 10^{-7}$ mbar at room temperature and $\approx 2 \times 10^{-8}$ mbar at low temperature). The temperature is controlled by two sensors: a carbon resistance and a compound linear thermal sensor (CLTS) situated on the holder, providing a precision of 0.1 K.

The column density (initially $N_0 = 1.5 \times 10^{18}$ molecules/cm^2) was estimated from the first order relation

$$N = \frac{1}{A} \int \tau_\upsilon d\upsilon \qquad (1)$$

where $A = 7.6 \times 10^{17}$ cm/molecule (Gerakines et al. 1995) is the CO_2 integrated absorbance of the ν_3 stretching mode (2343 cm^{-1}), and the integral of optical depth (τ_υ) over the frequency range is in practice the band area of the peak multiplied by 2.303. The thickness (0.66 μm) is obtained from the initial column density multiplied by molar mass (48 g/mol) divided by density (1.82 g/cm^3; Ponciano et al. 2006) and Avogadro's number. The deposition rate was of the order of 2 μm/h.

Table 1. Peak position and assignments for unirradiated $C^{18}O_2$ ice.

Position (cm^{-1})	Assignment
3627[1]	$2\nu_2 + \nu_3$
3518[1]	$\nu_1 + \nu_3$
2311	ν_3
2247	ν_3; $^{13}C^{18}O_2$
650	ν_2

[1] Fermi resonance.

The substrate was first cooled to 12–13 K. The system can be turned over 180° and fixed in three different positions to allow: i) gas deposition (through the needle valve), ii) the FTIR measurement (IR beam); and iii) perpendicular irradiation (ion beam) as shown in Fig. 2. Infrared spectra were measured using a Nicolet FTIR spectrometer (Magna 550) at a 1 cm^{-1} spectral resolution in the 5000–600 cm^{-1} (2–16.7 μm) region. The spectra are corrected by a background level collected before gas deposition. Spectra are collected at different fluences up to 1.5×10^{13} particles/cm^2. This allows us to observe the evolution of destruction and formation of molecules in the ice. The ion flux was about 2×10^9 cm^{-2} s^{-1}. For such a high flux experiment, an increase of temperature of approximately 0.5 K was observed after 3 h of irradiation (which corresponds to the maximum fluence of 1.5×10^{13} particles/cm^2).

The electronic and nuclear stopping powers predicted by SRIM (Ziegler & Biersack 2006) are 2.6×10^3 eV/(10^{15} molecules/cm^2) and 8.7 eV/(10^{15} molecules/cm^2), respectively, for the 46 MeV $^{58}Ni^{11+}$ ion beam. Note that this electronic stopping power is close to the maximum possible energy loss for an Ni projectile.

3. Results and discussion

IR spectra of both unirradiated and irradiated $C^{18}O_2$ are shown in Fig. 3 in the 4500–600 cm^{-1} region. The position of the $C^{18}O_2$ observed lines and its associated assignments are presented in Table 1. New lines appeared in the IR spectra due to ion irradiation. The main lines are associated with the ν_1 vibration of CO molecules at 2140 cm^{-1} (^{16}O) and 2088 cm^{-1} (^{18}O). The bands of O_3, C_3 and CO_3 molecules are also observed at 989 cm^{-1}, 2039 cm^{-1} and 2008 cm^{-1}, respectively. These radiolysis products present a maximum column density at 2.5×10^{12} ions cm^{-2} except CO_3 for which the maximum occurs at 5.0×10^{11} ions cm^{-2} (Fig. 4).

The band areas were measured and converted to column densities using Eq. (1). These values and the corresponding maximum column densities for the species identified in this work are presented in Table 2. After a 1.5×10^{13} ions cm^{-2} fluence, these lines disappear, indicating that the sputtering effect of the incoming projectile is important.

Figure 5 presents the evolution of the CO_2 column density as a function of fluence. The figure presents two regimes: the first one for $F < 10 \times 10^{12}$ cm^{-2}, and the second one above this value.

3.1. First regime

For this regime, two approaches were used to understand which processes occur during irradiation. In the first model, the projectile breaks the molecules and their fragments stay inside the ice. In this case, the CO_2 column density varies exponentially as a function of fluence (Fig. 5, curve a). The obtained destruction cross section is 2.2×10^{-13} cm^2. At low fluences, the

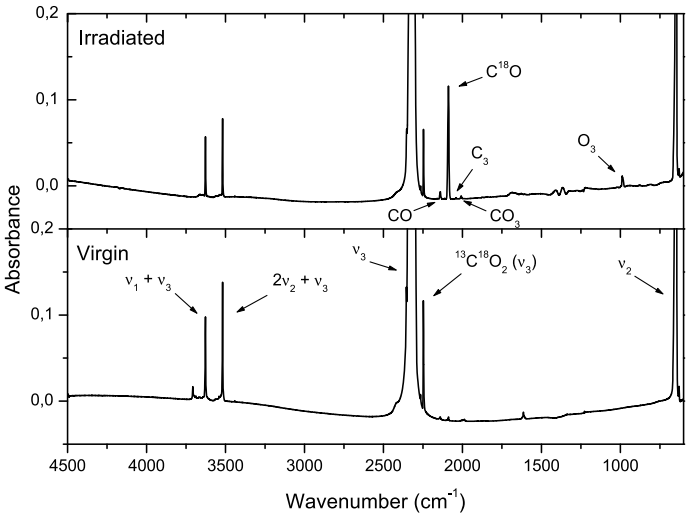

Fig. 3. $C^{18}O_2$ spectra before (*bottom*) and after (*top*) the irradiation of 2.5×10^{12} ions cm^{-2}. The unirradiated the spectrum was shifted by 0.2 on the vertical axis.

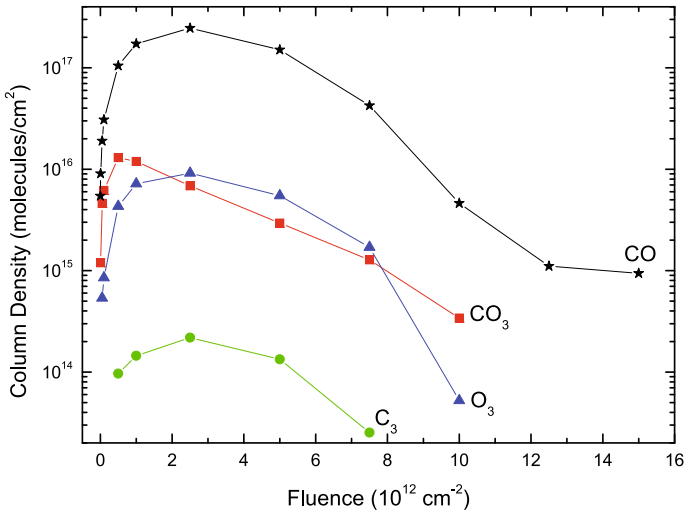

Fig. 4. Column density of $C^{18}O$, $C^{18}O_3$, C_3 and $^{18}O_3$ molecules as a function of fluence.

data and the fit are in good agreement, showing that the CO_2 destruction is obviously the main physical process. However, for $F > 5.0 \times 10^{12}$ cm^{-2}, the column density deviates from exponential behavior. This indicates the existence of a second process. In heavy ion irradiation of materials, sputtering is an important effect (Toulemonde et al. 2003) leading to sputtering yields as high as up to 10^5 atoms per incoming ion in the electronic sputering regime. In the second model studied, sputtering was included and the differential equation describing the column density variation as a function of fluence (dN_1/dF) is

$$dN_1/dF = -\sigma_{d1} N_1 - Y_1 \quad (2)$$

where σ_{d1} is the destruction cross section and Y_1 is the sputtering yield. Considering N_0 as the initial column density, the solution of this equation is

$$N_1 = N_0 \exp(-\sigma_{d1} F) - (Y_1/\sigma_{d1}) * (1 - \exp(-\sigma_{d1} F)). \quad (3)$$

Equation (3) was used to fit the evolution of the $C^{18}O_2$ column density (Fig. 5, curve b) for the first regime. For this fluence domain, the agreement between the experimental data and the fitting is excellent. The corresponding destruction

Table 2. Maximum column densities and the respective band strength for the species identified in this work.

Position (cm^{-1})	Molecule	N (10^{16} molecules cm^{-2})	Fluence (10^{12} cm^{-2})	A (10^{-17} cm molecule^{-1})	Reference
2311	$C^{18}O_2$	150	0	7.6	Gerakines et al. (1995)
2088	$C^{18}O$	25	2.5	1.1	Gerakines et al. (1995)
2039	C_3	0.022	2.5	10	Hutter et al. (1994)
2008	$C^{18}O_3$	1.3	0.5	0.54	Gerakines et al. (1996)
989	$^{18}O_3$	0.9	2.5	1.5	Bennet et al. (2005)

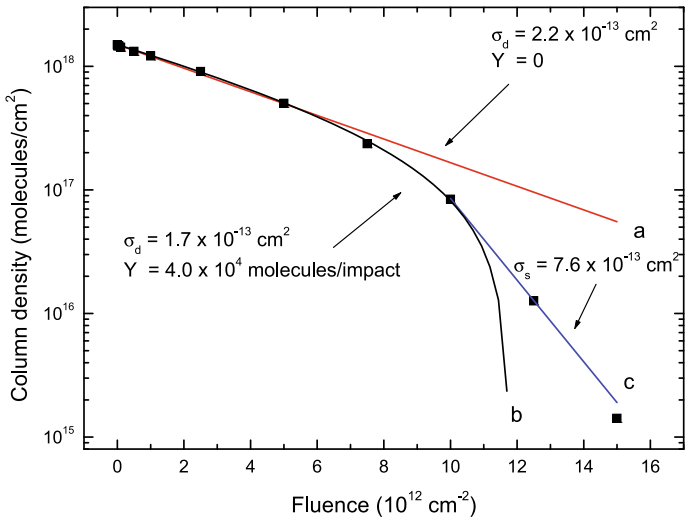

Fig. 5. Column density of $^{12}C^{18}O_2$ molecule as a function of fluence calculated from the absorbance 2311 cm^{-1} line. The data are fitted by Eq. (3) in the first regime and by $N_{min}\exp(-\sigma_s F)$ in the second regime (for details see in the text).

cross section and sputtering yield are 1.7×10^{-13} cm^2 and 4.0×10^4 molecules/impact, respectively. The yield obtained in the present work has a quadratic dependence on the electronic stopping power, as observed by Brown et al. (1982) for CO_2. The sputtering yield induced by protons of 0.8 MeV/u is nearly 4 orders of magnitude lower (approximately 3 molecules/impact; Brown et al. 1982).

The interaction between a fast heavy ion and an ice target is complex and partial scenarios may be set up by considering successive aspects of the phenomenon. Since we are in the electronic energy loss domain, most of the deposited energy leads to excitation of target electrons. In turn, the electrons thus liberated transfer their kinetic energy to the surrounding condensed molecules. The re-neutralization of the track proceeds concomitantly with the local temperature rise, leading to an eventual sublimation. A first approach consists of considering that all the energy lost by the projectile to the target is driven uniquely into thermal motion. For a given ice volume $V = S \times \Delta x$ (S being the track area) heated by the beam, the (homogenously) transferred energy can be written as

$$(\mathrm{d}E/\mathrm{d}x)\Delta x = \rho V(c\Delta T + C_L) \quad (4)$$

where $\mathrm{d}E/\mathrm{d}x$ is the total energy loss per unit path length of the projectile in ice, Δx is the heated ice thickness, ρ is ice density, ΔT is the temperature increase up to the sublimation temperature, c and C_L are the specific heat and latent heat, respectively. For the current system, the ice is initially at 13 K and $\Delta T = 72$ K is necessary for the CO_2 to reach the sublimation temperature at the base pressure. For 46 MeV Ni on $^{12}C^{18}O_2$, SRIM (Ziegler & Biersack 2006) predicts 6219 eV/nm and 21 eV/nm for the electronic and nuclear stopping powers. Considering $c = 0.84$ kJ/kg.K (Handbook 1996), $C_L = 200$ kJ/kg and $\rho = 1.82$ g/cm^3, it appears that the sublimation occurs over a cylinder around the projectile trajectory having a cross section of 2200 nm^2, corresponding to a radius of about 26 nm. Since the craters produced by MeV heavy ions are typically tens of nm deep (Schmidt et al. 1991), 10^5 molecules/impact is the order of magnitude expected for the thermal sputtering yield. Assuming that chemical reactions, ionization and molecular fragmentation could reduce the neutral desorption yield by one order of magnitude, a sputtering yield of 10^4 molecules/projectile is expected (which agrees with the value obtained above from the fitting procedure; Fig. 5 curve b). This agreement between the model and experimental data indicates that sputtering is connected to thermal processes.

3.2. Second regime

The second regime is interpreted as a failure of the $\mathrm{d}N_1/\mathrm{d}F = -Y$ condition, a consequence of the fact that the projectile is not impacting onto a CO_2 virgin region any longer. This occurs when the column density becomes lower than $N_{min} = 8.0 \times 10^{16}$ molecules/cm^2, attained for fluences higher than 1.0×10^{13} projectiles/cm^2. Under such conditions, the CO_2 ice thickness (660 nm, at the beginning of irradiation) decreases considerably and surface and bulk interactions cannot be treated independently. Y is not constant any longer and starts to be dependent on the column density of the CO_2, either because the density of new molecular species has become relatively high or because the ice surface is now too close to the substrate and the effects of projectile-substrate interaction can intervene. Since the second regime seems to exhibit an exponential decay, an "extra" cross section σ_s can be extracted from data to cover the mentioned overall effects. The fact that $\sigma_s > \sigma_d$ can be partially attributed to the increasing density of free radicals in the ice produced by the beam.

3.3. Formation of molecules

From the evolution of column density as a function of fluence (Fig. 4) the formation cross sections of CO, CO_3, and O_3 molecules were determined. Since at the beginning of the experiment the sputtering is negligible for these molecules, the main process occurring in the ice is the molecule formation. The corresponding cross sections can be then obtained directly from the slope of each curve from the first four points. The estimated cross sections are presented in Table 3.

CO molecule production has the highest cross section, showing that CO are the main species produced observable by FTIR spectroscopy; CO_2 dissociation occurs mainly via the $CO_2 \rightarrow CO + O$ pathway. The formation cross sections of the other molecules are one order of magnitude lower. In particular, the C_3 line was too weak to determine the associated cross

Table 3. Cross sections for the CO, O_3, CO_3, and C_3 molecule formation.

Molecules	σ_f (10^{-13} cm^2)
CO	1.6
O_3	0.15
CO_3	0.45
C_3	–

section. Therefore, carbonization, although it exists (Strazzulla et al. 2005), is of minor importance here.

4. Conclusions

^{18}O-labelled condensed CO_2 at 13 K was bombarded with 46 MeV $^{58}Ni^{11+}$. Irradiation causes formation of CO, O_3, CO_3, and C_3 molecules in the $\approx$0.66 μm thick CO_2 matrix. The ice essentially disappears after a fluence of 1.5×10^{13} particles/cm^2. From the present measurements, some relevant projectile-ice parameters were extracted: i) the total sputtering yield of 0.8 MeV/u Ni^{11+} on CO_2 ice is 4.0×10^4 molecules/impact; ii) the CO_2 destruction cross section is 1.7×10^{-13} cm^2; and iii) the CO, O_3, and CO_3 production cross sections are 1.6×10^{-13} cm^2, 1.5×10^{-14} cm^2, and 4.5×10^{-14} cm^2, respectively. Heavy ion cosmic rays, such as Fe and Ni ions, have an important role in sputtering of astrophysical ices.

Acknowledgements. The authors acknowledge the agencies COFECUB (France) as well as CAPES, CNPq and FAPERJ (Brazil) for partial support. It is a pleasure to thank E. Balanzat, Y. Ngono-Ravache, M. Ferry, and I. Monnet for technical assistance. Special thanks to A. Domaracka for carefully reading and commenting on the manuscript. In addition, the authors would like to acknowledge the referee for pertinent suggestions in order to improve this manuscript.

References

Allamandola, L. J., Bernstein, M. P., & Sandford, S. A. 1997, Proceedings of the 5th international conference on bioastronomy, IAU Coll., 161, 23
Baragaiola, R. A. 2005, Nucl. Instr. Meth. B, 232, 98
Baragiola, R. A., Fama, M., Loeffler, M. J., Raut, U., & Shi, J. 2008, Nucl. Instr. Meth. B, 266, 3057
Boezio, M., Carlson, P., Francke, T., et al. 1999, ApJ, 518, 457
Brena, B., Nordlund, D., Odelius, M., et al. 2004, Phys. Rev. Lett., 93, 14
Brown, W. L., Augustyniak, W. M., Simmons, et al. 1982, Nucl. Instr. Meth., 198, 1
van Broekhuizen, F. A., Groot, I. M. N., Fraser, H. J., van Dishoeck, E. F., & Schlemmer, S. 2006, A&A, 451, 723
Dartois, E. 2005, Space Sci. Rev., 119, 293
van Dishoeck, E. F. 2004, ARA&A, 42, 119
Ehrenfreund, P., Boorgert, A. C. A., Gerakines, P. A., et al. 1996, A&A, 315, L341
Falk, M. 1986, J. Chem. Phys., 86, 560
Farenzena, L. S., Isa, P., Martinez, et al. 2005, Earth, Moon, and Planets, 97, 311
Farenzena, L. S., Ponciano, C. R., da Silveira, E. F., & Wien, K. 2005, Int. J. Mass Spectrom., 243, 85
Farenzena, L. S., Martinez, R., Iza, P., et al. 2006, Int. J. Mass Spectrom., 251, 1
Gerakines, P. A., Schutte, W. A., Greenberg, J. M., & van Dishoeck, E. F. 1995, A&A, 296, 810
Gerakines, P. A., Schutte, W. A., & Ehrenfreund, P. 1996, A&A, 312, 289
Gerakines, P. A., Moore, M. H., & Hudson, R. L. 2000, A&A, 357, 793
Gibb, E. L., Whittet, D. C. B., Boogert, A. C. A., & Tielens, A. G. G. M. 2004, ApJS, 151, 35
Grim, R. J. A., Greenberg, J. M., de Groot, M. S., et al. 1989, A&AS, 78, 161
d' Hendecourt, L. B., & Allamandola, L. J. 1986, A&A, 64, 453
Handbook of Chemistry and Physics-CRC Press- Boca Raton, 1996
Hudson, R. L., & Moore, M. H. 1999, Icarus, 140, 451
Hutter, J., Lüthi, H. P., & Diederich, F. 1994, J. Am. Chem. Soc., 116, 750
Jamieson, C. S., Mebel, A. M., & Kaiser, R. I. 2006, ApJS, 163, 184
Jenniskens, P., & Blake, D. F. 1994, Science, 265, 753
Jones, A. 2000, Atomic and Molecular Data for Astrophysics: New Developments, Case Studies and Future Needs, 24th meeting of the IAU, Joint Discussion 1, August 2000, Manchester, England, meeting abstract., 1,
Jones, A. P., Tielens, A. G. G. M., & Hollenbach, D. J. 1996, ApJ, 469, 740
Karrer, R., Bochsler, P., Giammanco, C., et al. 2007, Space Sci. Rev., 130, 317
Lafosse, A., Bertin, M., Domaracka, A., et al. 2006, Phys. Chem. Chem. Phys., 8, 5564
Loeffler, M. J., Baratta, G. A., Palumbo, M. E., Strazzulla, G., & Baragiola, R. A. 2005, A&A, 435, 587
Mewaldt, R. A., Cohen, C. M. S., Mason, G. M., Haggerty, D. K., & Desai, M. I. 2007, Space Sci. Rev., 130, 323
Moore, M. H., Khanna, R., & Donn, B. 1991, J. Geophys. Res., 96, 17541
Palumbo, M. E., Baratta, G. A., Brucato, J. R., et al. 1998, A&A, 334, 247
Pinchas, S., & Laulicht, I. 1971, Infrared Spectra of Labelled Compounds (London and New York: Academic Press)
Ponciano, C. R., Farenzena, L. S., Collado, V. M., da Silveira, E. F., & Wien, K. 2005, Int. J. Mass Spectrom., 244, 41
Ponciano, C. R., Martinez, R., Farenzena, L. S., et al. 2006, J. Am. Mass Spectrom., 17, 1120
Ponciano, C. R., Martinez, R., Farenzena, et al. 2008, J. Mass Spectrom., 43, 1521
Pontoppidan, K. M., Boogert, A. C. A., Fraser, H. J., et al. 2008, ApJ, 678, 1005P
Roser, J. E., Vidali, G., Manicò, G., & Pirronello, V. 2001, ApJ, 555, 61
Schmidt, R., Schoppmann C., Brandl, D., et al. 1991, Phys. Rev. B, 44, 2.
Shen, C. J., Greenberg, J. M., Schutte, W. A., & van Dishoeck, E. F. 2004, A&A, 415, 203
Strazzulla, G., Leto, G., LaDelfa, S., Spinella, F., & Gomis, O. 2005, Mem. S. A. It. Suppl., 6, 51
Toulemonde, M., Assmann, W., Trautmann, C., et al. 2003, Nucl. Instr. Meth. Phys. Res. Sec. B, 212, 346
Webber, W. R., & Yushak, S. M. 1983, ApJ, 275, 391
Whittet, D. C. B., Shenoy, S. S., Bergin, E. A., et al. 2007, ApJ, 655, 332
Wood, B. E., & Roux, J. A. 1982, J. Opt. Soc. Am., 72, 720
Ziegler, J. F., & Biersack, J. P. 2006, http://www.srim.org, version 2006.02